Palestine Journal of Mathematics

Vol.15(3), (2026) , 395–413 © Palestine Polytechnic University-PPU 2026

Topological Entropy and Numerical Methods for Nonlinear Volterra–Fredholm Integral Equations: Finite Difference and Spectral Approaches

Karrar S.Abed and Ahmed M.Rajab

Communicated by Geeta Arora

MSC 2020 Classifications: Primary 45G10; Secondary 65M06, 37B40, 65M12.

Keywords and phrases: topological entropy, finite difference method, nonlinear Volterra-Fredholm integral equations, numerical stability, chaos detection, discretization error..

The authors would like to thank the reviewers and editor for their constructive comments and valuable suggestions that improved the quality of our paper.

Corresponding Author: Ahmed M. Rajab

Abstract This paper examines the relationship between topological entropy and numerical dissection techniques, particularly the finite-difference method, for solving nonlinear Volterra-Fredholm integral equations . We first establish a theoretical framework for topological entropy in the context of dynamical integral systems resulting from these equations. We then develop and analyze a finite-difference scheme for numerically approximating solutions to these equations. We rigorously prove the convergence and stability of the method. We then explore how topological entropy can be a measure of complexity and sensitivity in the solution space, and how it relates to the numerical error and dissection step size. Numerical experiments illustrate the theoretical results and demonstrate the effectiveness of the proposed method. This study bridges abstract dynamical systems theory with practical numerical analysis, providing new insights into the behavior of solutions to nonlinear integral equations.

1 Introduction

Nonlinear Volterra-Fredholm integral equations (VFIEs) represent a powerful and versatile class of functional equations that combine the causal, memory-dependent structure of Volterra operators with the global, boundary-influenced nature of Fredholm operators. These equations naturally arise in modeling physical, biological, and engineering systems where both temporal evolution and spatial or parametric averaging are simultaneously at play for instance, in age-structured population dynamics with migration [4], nonlocal heat conduction [8], electromagnetic wave scattering [7], and optimal control of distributed parameter systems [15]. The presence of nonlinearity further complicates the solution landscape, potentially giving rise to phenomena such as bifurcations, multistability, and even chaotic dynamics features that render traditional analytical methods inadequate and [18] pose significant challenges for numerical approximation .

While substantial progress has been made in developing numerical techniques including collocation, Galerkin, wavelet, and quadrature-based methods the convergence and stability of these schemes often hinge critically on the regularity and contractivity of the kernel functions. More fundamentally, in cases where the integral operator induces complex or sensitive dynamics, classical error estimates based on smoothness or Lipschitz constants may fail to capture the true numerical behavior. Discretization errors may amplify unpredictably, iterative solvers may stagnate or diverge, and solution trajectories may exhibit high sensitivity to initial guesses or grid resolution. This reveals a gap in the current numerical analysis toolkit: a lack of *complexity-aware* diagnostics that go beyond normed error bounds to quantify the intrinsic structural richness and instability of the underlying operator dynamics.

Topological entropy a concept originally introduced by Adler, Konheim, and McAndrew [1]

and later refined by Bowen [2] for maps on compact spaces offers precisely such a diagnostic. It quantifies the exponential growth rate of distinguishable orbits under iteration, serving as a rigorous measure of unpredictability, information generation, and dynamical complexity. Although traditionally applied to finite-dimensional maps and flows, recent developments have extended its applicability to infinite-dimensional systems, including those governed by integral and integro-differential equations [17, 10, 6]. Yet, its use in the context of *numerical discretization* of integral equations particularly as a predictor of computational difficulty remains largely unexplored.

In this paper, we bridge this theoretical-computational divide by introducing topological entropy as a practical tool for analyzing and predicting the behavior of finite difference methods applied to nonlinear VFIEs. Our work makes the following contributions:

(i) We formulate and analyze a finite difference scheme based on composite quadrature rules for discretizing nonlinear VFIEs. Under Lipschitz-type assumptions on the kernels, we prove convergence and derive explicit stability conditions that relate step size to kernel constants.

(ii) We adapt the notion of topological entropy to discrete numerical trajectories generated by iterative solution of the discretized system. We propose a computable entropy estimator based on symbolic dynamics, where the solution space is partitioned and trajectories are encoded into symbol sequences whose growth rate approximates the entropy.

(iii) Through carefully designed numerical experiments, we demonstrate a strong empirical correlation between estimated topological entropy and key numerical indicators: convergence rate, iteration count, and discretization error. High entropy consistently corresponds to slower convergence, greater sensitivity to grid refinement, and increased risk of solver failure suggesting entropy can serve as an *a priori* indicator of numerical tractability and a guide for adaptive method selection.

This study sits at the intersection of numerical analysis, dynamical systems theory, and scientific computing. It extends recent theoretical work on entropy for infinite-dimensional systems [10, 6] by embedding it within a concrete computational framework. More broadly, it proposes a paradigm shift: rather than viewing entropy as a purely abstract invariant, we treat it as a quantifiable, computable property with direct implications for algorithm design and performance prediction.

While the authors have previously studied spectral methods for fractional integro-differential equations [18], the application of topological entropy to analyze solver dynamics for nonlinear Volterra–Fredholm integral equations represents a new direction. Specifically, our earlier work focused on adaptive Chebyshev-Gauss-Lobatto discretizations for nonsmooth solutions of Caputo-type initial value problems, with emphasis on error estimation and grid refinement. In contrast, the present manuscript addresses a distinct class of problemsnonlinear integral equations with both Volterra and Fredholm terms and introduces a dynamical systems perspective by quantifying the complexity of iterative solvers through numerical entropy. This shift enables a novel comparison between finite difference and spectral methods not based solely on accuracy, but on the intrinsic predictability and stability of their solution trajectories.

The remainder of this paper is organized as follows. Section 2 introduces the mathematical formulation of nonlinear VFIEs and reviews the definition of topological entropy in the context of integral operators. Section 3 details the finite difference discretization scheme and provides rigorous proofs of convergence and stability. Section 4 develops a spectral approximation method based on Legendre polynomials and establishes error estimates in both L^2 and L^∞ norms.Section 5 describes our procedure for estimating entropy from numerical solutions and discusses its relationship to discretization parameters. Section 6 presents numerical experiments that validate our theoretical claims and illustrate the predictive power of entropy. Finally, Section 7 concludes with a summary of findings and outlines promising directions for future research.

2 Mathematical Preliminaries

2.1 Nonlinear Volterra-Fredholm Integral Equations

Consider the following nonlinear Volterra-Fredholm integral equation:

$$u(x) = f(x) + \int_0^x K_1(x,t,u(t))\,dt + \int_0^1 K_2(x,t,u(t))\,dt, \quad x \in [0,1], \tag{2.1}$$

where $f \in C[0,1]$ is a given continuous function, and the kernels $K_1, K_2 : [0,1]\times[0,1]\times\mathbb{R} \to \mathbb{R}$ are continuous and nonlinear.

We assume the kernels satisfy global Lipschitz conditions in their third argument:

$$|K_i(x,t,u) - K_i(x,t,v)| \le L_i|u-v|, \quad i = 1,2,$$

for some constants $L_1, L_2 > 0$. These conditions ensure that the associated integral operator is contractive on a suitable subset of $C[0,1]$, guaranteeing existence and uniqueness of solutions via Banach's fixed point theorem.

Definition 2.1 (Integral Operator T).
Let $C[0,1]$ denote the Banach space of continuous real-valued functions on $[0,1]$ equipped with the supremum norm $\|\cdot\|_\infty$. Given $f \in C[0,1]$ and continuous kernels $K_1, K_2 : [0,1]^2 \times \mathbb{R} \to \mathbb{R}$, define the nonlinear operator $T : C[0,1] \to C[0,1]$ by

$$(Tu)(x) = f(x) + \int_0^x K_1(x,t,u(t))\,dt + \int_0^1 K_2(x,t,u(t))\,dt.$$

A solution $u \in C[0,1]$ to the Volterra-Fredholm integral equation (2.1) is a fixed point of T, i.e., $Tu = u$. Under the Lipschitz conditions stated above, T becomes a contraction on a suitable closed ball in $C[0,1]$, ensuring existence and uniqueness of solutions [4, 8].

2.2 Topological Entropy for Integral Operators

Definition 2.2 (Topological Entropy of a Continuous Map).
Let (X,d) be a compact metric space and $T : X \to X$ a continuous map. For $n \in \mathbb{N}$ and $\varepsilon > 0$, a finite set $E \subset X$ is called (n,ε)-*separated* if for every pair of distinct points $x, y \in E$, there exists an integer k with $0 \le k < n$ such that $d(T^k x, T^k y) > \varepsilon$. Let $s(n,\varepsilon,T)$ denote the maximum cardinality of such a set. The *topological entropy* of T is defined as

$$h_{\text{top}}(T) = \lim_{\varepsilon\to 0^+} \limsup_{n\to\infty} \frac{1}{n} \log s(n,\varepsilon,T).$$

This measures the exponential growth rate of distinguishable orbit segments and quantifies the complexity of the dynamical system (X,T) [1, 2, 13].

Remark 2.3.
Although $C[0,1]$ is not compact in the uniform topology, we can construct a compact invariant set as follows. Let

$$M := \|f\|_\infty + \frac{L_1+L_2}{1-(L_1+L_2)} \cdot \sup_{x\in[0,1]} \left(|K_1(x,x,0)| + |K_2(x,1,0)|\right),$$

assuming $L_1 + L_2 < 1$ (so the denominator is positive). Define the closed ball

$$\mathcal{B} := \left\{u \in C[0,1] : \|u\|_\infty \le M\right\}.$$

To ensure equicontinuity, observe that for any $u \in \mathcal{B}$ and $x, y \in [0,1]$ with $x < y$,

$$|Tu(x) - Tu(y)| \le |f(x) - f(y)| + \left|\int_0^x K_1(x,t,u(t))\,dt - \int_0^y K_1(y,t,u(t))\,dt\right| + \left|\int_0^1 \left(K_2(x,t,u(t)) - K_2(y,t,u(t))\right)dt\right|.$$

Since f, K_1, and K_2 are continuous on compact domains, they are uniformly continuous. Moreover, the Lipschitz condition in the third argument and the uniform bound $|u(t)| \leq M$ imply that the integrands are uniformly bounded and equicontinuous in x. Thus, $T(\mathcal{B})$ is equicontinuous.

Furthermore, for any $u \in \mathcal{B}$,

$$\begin{aligned}\|Tu\|_\infty &\leq \|f\|_\infty + \sup_{x\in[0,1]} \int_0^x |K_1(x,t,u(t))|\,dt + \sup_{x\in[0,1]} \int_0^1 |K_2(x,t,u(t))|\,dt \\ &\leq \|f\|_\infty + \sup_{x,t} |K_1(x,t,0)| + L_1\|u\|_\infty + \sup_{x,t} |K_2(x,t,0)| + L_2\|u\|_\infty \\ &\leq \|f\|_\infty + C_0 + (L_1+L_2)M,\end{aligned}$$

where $C_0 = \sup_{x,t}(|K_1(x,t,0)| + |K_2(x,t,0)|)$. Choosing M such that

$$M \geq \|f\|_\infty + C_0 + (L_1+L_2)M,$$

i.e.,

$$M \geq \frac{\|f\|_\infty + C_0}{1-(L_1+L_2)},$$

ensures $\|Tu\|_\infty \leq M$, so $T(\mathcal{B}) \subset \mathcal{B}$.

Since $\mathcal{B}$ is closed, bounded, and equicontinuous, its closure $\overline{\mathcal{B}}$ is compact by the Arzelà–Ascoli theorem. The invariance $T(\overline{\mathcal{B}}) \subset \overline{\mathcal{B}}$ follows from continuity of T. Hence, the restriction $T|_{\overline{\mathcal{B}}}$ is a continuous self-map on a compact metric space, and its topological entropy $h_{\text{top}}(T|_{\overline{\mathcal{B}}})$ is well-defined. This construction is standard in the analysis of infinite-dimensional dynamical systems generated by integral operators [10, 17].

Remark 2.4.
Although $C[0,1]$ is not compact in the uniform topology, we may restrict T to a closed, bounded, and equicontinuous subset $\mathcal{B} \subset C[0,1]$, which by the Arzelà–Ascoli theorem is precompact. If $T(\mathcal{B}) \subset \mathcal{B}$, then the closure $\overline{\mathcal{B}}$ is compact and invariant, allowing $h_{\text{top}}(T|_{\overline{\mathcal{B}}})$ to be well-defined. This framework is standard in the study of infinite-dimensional dynamical systems generated by integral operators [10, 17].

Let $T : C[0,1] \to C[0,1]$ be the integral operator defined by the right-hand side of (2.1). We consider the discrete dynamical system generated by iterating T:

$$u_{n+1} = T(u_n), \quad n = 0,1,2,\ldots$$

The topological entropy $h_{\text{top}}(T)$ measures the asymptotic growth of orbit complexity under this iteration.

In practice, for numerical computation, we approximate $h_{\text{top}}(T)$ using the growth rate of distinct symbolic sequences generated by discretized trajectories. This approach, grounded in symbolic dynamics, allows us to estimate entropy from finite-precision numerical simulations a key step in linking abstract dynamical systems theory with computational analysis.

3 Finite Difference Method for VFIEs

3.1 Discretization Scheme

Let $x_i = ih$ for $i = 0,1,\ldots,N$, where $h = 1/N$, and denote the numerical approximation to $u(x_i)$ by u_i. The integrals in (2.1) are approximated using the composite trapezoidal rule:

$$\int_0^{x_i} K_1(x_i,t,u(t))\,dt \approx h\sum_{j=0}^{i} w_{ij}^{(1)} K_1(x_i,x_j,u_j),$$

$$\int_0^{1} K_2(x_i,t,u(t))\,dt \approx h\sum_{j=0}^{N} w_{ij}^{(2)} K_2(x_i,x_j,u_j),$$

where the weights $w_{ij}^{(1)}$ and $w_{ij}^{(2)}$ are defined by

$$w_{ij}^{(1)} = \begin{cases} \frac{1}{2}, & \text{if } j = 0 \text{ or } j = i, \\ 1, & \text{if } 1 \le j \le i-1, \end{cases} \qquad w_{ij}^{(2)} = \begin{cases} \frac{1}{2}, & \text{if } j = 0 \text{ or } j = N, \\ 1, & \text{if } 1 \le j \le N-1. \end{cases}$$

The resulting discrete system is then given by

$$u_i = f(x_i) + h\sum_{j=0}^{i} w_{ij}^{(1)} K_1(x_i, x_j, u_j) + h\sum_{j=0}^{N} w_{ij}^{(2)} K_2(x_i, x_j, u_j), \quad i = 0, 1, \ldots, N. \tag{3.1}$$

These weights correspond to the standard composite trapezoidal rule and ensure second-order accuracy for sufficiently smooth integrands.

Lemma 3.1 (Discrete Lipschitz Continuity of T_h).
Let $\mathbf{u}, \mathbf{v} \in \mathbb{R}^{N+1}$ and let $T_h : \mathbb{R}^{N+1} \to \mathbb{R}^{N+1}$ be the discrete operator defined by the finite difference scheme (3.1). Assume the kernels K_1, K_2 satisfy global Lipschitz conditions:

$$|K_i(x,t,u) - K_i(x,t,v)| \le L_i|u - v|, \quad i = 1, 2, \quad \forall x, t \in [0,1],\ u, v \in \mathbb{R}.$$

Then the operator T_h satisfies

$$\|T_h\mathbf{u} - T_h\mathbf{v}\|_\infty \le (L_1 + L_2)\|\mathbf{u} - \mathbf{v}\|_\infty.$$

Consequently, if $L_1 + L_2 < 1$, then T_h is a contraction on $\mathbb{R}^{N+1}$ under the max norm, uniformly in h.

Proof.
For each grid point x_i, we estimate:

$$\begin{aligned} |(T_h\mathbf{u})_i - (T_h\mathbf{v})_i| &\le hL_1 \sum_{j=0}^{i} w_{ij}^{(1)}|u_j - v_j| + hL_2 \sum_{j=0}^{N} w_{ij}^{(2)}|u_j - v_j| \\ &\le hL_1\|\mathbf{u} - \mathbf{v}\|_\infty \sum_{j=0}^{i} w_{ij}^{(1)} + hL_2\|\mathbf{u} - \mathbf{v}\|_\infty \sum_{j=0}^{N} w_{ij}^{(2)}. \end{aligned}$$

By the exactness of the composite trapezoidal rule on uniform grids,

$$h\sum_{j=0}^{i} w_{ij}^{(1)} = x_i \le 1, \qquad h\sum_{j=0}^{N} w_{ij}^{(2)} = 1.$$

Hence,

$$|(T_h\mathbf{u})_i - (T_h\mathbf{v})_i| \le (L_1 + L_2)\|\mathbf{u} - \mathbf{v}\|_\infty.$$

Taking the supremum over $i = 0, \ldots, N$ yields the result. □

Theorem 3.2 (Convergence and Error Estimate for Iterative Scheme).
Suppose the conditions of Lemma 3.1 hold and that h is chosen small enough so that $\alpha(h) = (L_1 + L_2)(1 + h/2) < 1$. Then:

(i) The discrete operator T_h has a unique fixed point $\mathbf{u}^* \in \mathbb{R}^{N+1}$.

(ii) For any initial guess $\mathbf{u}^{(0)}$, the iterative sequence $\mathbf{u}^{(k+1)} = T_h(\mathbf{u}^{(k)})$ converges to $\mathbf{u}^*$.

(iii) The error at the k-th iteration satisfies

$$\|\mathbf{u}^{(k)} - \mathbf{u}^*\|_\infty \le \frac{\alpha(h)^k}{1 - \alpha(h)}\|\mathbf{u}^{(1)} - \mathbf{u}^{(0)}\|_\infty.$$

Proof.
Part (i) and (ii) follow directly from the Banach Fixed-Point Theorem applied to the complete metric space $(\mathbb{R}^{N+1}, \|\cdot\|_\infty)$ [3, Theorem 5.1.1]. The error estimate in (iii) is a standard consequence of contraction mapping theory; see [10, Proposition 1.1] or [14, Lemma 2.2]. □

Corollary 3.3.
If $L_1 + L_2 < 1$, then any step size $h < \frac{2(1-L_1-L_2)}{L_1+L_2}$ guarantees convergence of the iterative scheme.

Proof.
Recall from Lemma 3.1 that the discrete operator T_h satisfies

$$\|T_h\mathbf{u} - T_h\mathbf{v}\|_\infty \leq \alpha(h)\|\mathbf{u} - \mathbf{v}\|_\infty,$$

where

$$\alpha(h) = (L_1 + L_2)\left(1 + \frac{h}{2}\right). \tag{3.2}$$

By Theorem 3.2, the iterative scheme converges if $\alpha(h) < 1$.

Assume $L_1 + L_2 < 1$. We seek the largest $h > 0$ such that $\alpha(h) < 1$. Solving the inequality:

$$(L_1 + L_2)\left(1 + \frac{h}{2}\right) < 1.$$

Divide both sides by $L_1 + L_2$ (which is positive):

$$1 + \frac{h}{2} < \frac{1}{L_1 + L_2}.$$

Subtract 1 from both sides:

$$\frac{h}{2} < \frac{1}{L_1 + L_2} - 1 = \frac{1 - (L_1 + L_2)}{L_1 + L_2}.$$

Multiply both sides by 2:

$$h < \frac{2(1 - L_1 - L_2)}{L_1 + L_2}.$$

Thus, for any step size h satisfying this bound, we have $\alpha(h) < 1$, and hence T_h is a contraction on $\mathbb{R}^{N+1}$. By the Banach Fixed-Point Theorem [3, Theorem 5.1.1], the iterative scheme converges to the unique fixed point for any initial guess. □

Remark 3.4 (Practical Interpretation of the Step-Size Restriction).
The step-size condition $h < \frac{2(1-L_1-L_2)}{L_1+L_2}$ is derived from the conservative estimate $\alpha(h) = (L_1+L_2)(1+h/2)$, which overestimates the true Lipschitz constant of the discrete operator (see discussion in Section 3). In reality, the composite trapezoidal rule satisfies $h\sum w_{ij}^{(1)} = x_i \leq 1$ and $h\sum w_{ij}^{(2)} = 1$, so the sharp bound is $\alpha = L_1 + L_2$, independent of h.

Consequently, if $L_1 + L_2 < 1$, the iterative scheme converges for any $h > 0$ (i.e., for any N), and the step-size restriction in Corollary 3.3 is an artifact of the proof technique rather than a practical limitation. This is confirmed in our numerical experiments (Section 6), where convergence is observed even for large h (coarse grids) as long as $L_1 + L_2 < 1$.

Thus, the essential requirement is the global contractivity of the continuous operator, not a small step size. The corollary's bound should be viewed as a theoretical safeguard under a loose estimate, not a design constraint in practice.

3.2 Iterative Solution

We solve (3.1) iteratively. Let $u_i^{(0)}$ be an initial guess (e.g., $u_i^{(0)} = f(x_i)$). Then for $k = 0, 1, \ldots$ until convergence:

$$u_i^{(k+1)} = f(x_i) + h\sum_{j=0}^{i} w_{ij}^{(1)} K_1(x_i, x_j, u_j^{(k)}) + h\sum_{j=0}^{N} w_{ij}^{(2)} K_2(x_i, x_j, u_j^{(k)}).$$

4 Spectral Approximation Using Legendre Polynomials and Error Analysis

In addition to finite difference methods, spectral methods based on orthogonal polynomials offer high-order (often exponential) accuracy for smooth solutions of integral equations. In this section, we apply a Legendre–Galerkin spectral method to the nonlinear Volterra–Fredholm integral equation (2.1) and analyze its convergence and dynamical properties.

Let $\mathbb{P}_N[0,1]$ denote the space of polynomials of degree at most N on $[0,1]$, and let $\{\tilde{L}_k(x)\}_{k=0}^N$ be the shifted Legendre polynomials, orthogonal with respect to the L^2 inner product on $[0,1]$. We seek an approximate solution $u_N \in \mathbb{P}_N[0,1]$ of the form

$$u_N(x) = \sum_{k=0}^{N} \hat{u}_k \tilde{L}_k(x),$$

where the coefficients $\{\hat{u}_k\}$ are determined by enforcing a Galerkin weak formulation of (2.1).

The following theorem summarizes the approximation properties of this scheme.

Theorem 4.1 (Spectral Convergence). *Assume the exact solution u of (2.1) belongs to $H^m(0,1)$ for some $m \geq 1$, and that the kernels K_1, K_2 are Lipschitz continuous and sufficiently smooth. Then the Legendre–Galerkin approximation u_N satisfies*

$$\|u - u_N\|_{L^2(0,1)} \leq CN^{-m}, \qquad \|u - u_N\|_{L^\infty(0,1)} \leq CN^{1/2-m}.$$

Moreover, if u is analytic in a neighborhood of $[0,1]$, then the convergence is exponential: there exist constants $C, \sigma > 0$ such that

$$\|u - u_N\|_{L^\infty(0,1)} \leq Ce^{-\sigma N}.$$

This result follows from classical spectral approximation theory; a detailed proof is provided in Appendix A.1.

A remarkable consequence of this rapid convergence is the simplification of the solver dynamics at high resolution. Let $\{u_N^{(k)}\}_{k=0}^M$ denote the sequence of iterates generated by the nonlinear solver in coefficient space, and let $h_{\text{num}}(N)$ denote the estimated topological entropy of this trajectory .

Theorem 4.2 (Exponential Entropy Decay). *If the exact solution u is analytic and the discrete iteration map is contractive, then the numerical entropy decays exponentially with N:*

$$h_{\text{num}}(N) \leq Ce^{-\sigma N}, \quad \textit{for some } C, \sigma > 0.$$

The proof, based on the exponential decay of residuals and the contraction properties of the discrete operator, is given in Appendix A.2.

This entropy decay directly impacts solver efficiency:

Corollary 4.3 (Bounded Iteration Count). *Under the assumptions of Theorem 4.2, the number of iterations $K(N)$ required to achieve a fixed tolerance $\varepsilon > 0$ satisfies*

$$K(N) = \mathcal{O}\left(\frac{1}{N}\right) \quad \textit{as } N \to \infty.$$

In particular, $K(N)$ remains uniformly bounded and typically decreases as N increases.

A complete derivation of this bound, including asymptotic analysis of the Lipschitz constant $\alpha(N)$, is provided in Appendix A.3.

Finally, we compare the dynamical complexity of spectral and finite difference discretizations:

Proposition 4.4 (Entropy: Spectral vs. Finite Difference). *Let $h_{\text{num}}^{\text{FD}}(h)$ and $h_{\text{num}}^{\text{Spec}}(N)$ denote the numerical entropies for finite difference (step size h) and spectral (degree N) approximations of comparable accuracy, i.e., $\|u - u_h\|_\infty \approx \|u - u_N\|_\infty$. If u is smooth, then for sufficiently small h and large N,*

$$h_{\text{num}}^{\text{Spec}}(N) < h_{\text{num}}^{\text{FD}}(h).$$

The proof, which combines dimensionality, regularity, and sensitivity arguments, is given in Appendix A.4.

Remark 4.5. This analysis reveals a key advantage of spectral methods for smooth nonlinear problems: not only do they converge faster, but their iterative solution dynamics become *simpler* (lower entropy) as resolution increasesmaking high-degree approximations computationally favorable.

5 Topological Entropy and Numerical Solutions

5.1 Entropy Estimation from Discrete Trajectories

Given a sequence of numerical solutions $\{\mathbf{u}^{(k)}\}_{k=0}^{M} \subset \mathbb{R}^{N+1}$ generated by the iterative scheme $\mathbf{u}^{(k+1)} = T_h(\mathbf{u}^{(k)})$, we estimate the topological entropy by encoding the trajectory into a symbolic sequence. To this end, we first determine the empirical range of the solution components across all iterates:

$$u_{\min} = \min_{\substack{0\le k\le M\\ 0\le i\le N}} u_i^{(k)}, \qquad u_{\max} = \max_{\substack{0\le k\le M\\ 0\le i\le N}} u_i^{(k)}.$$

We then partition the interval $[u_{\min}, u_{\max}]$ into $r \ge 2$ subintervals of equal length:

$$I_s = [u_{\min} + (s-1)\Delta,\ u_{\min} + s\Delta)\,, \quad s = 1, \dots, r-1, \qquad I_r = [u_{\min} + (r-1)\Delta,\ u_{\max}]\,,$$

where $\Delta = (u_{\max} - u_{\min})/r$. Each component $u_i^{(k)}$ is assigned a symbol $s \in \{1, \dots, r\}$ such that $u_i^{(k)} \in I_s$. This yields a joint symbolic state $\phi(\mathbf{u}^{(k)}) \in \{1, \dots, r\}^{N+1}$ at each iteration k, and the full trajectory is represented by the sequence

$$\big(\phi(\mathbf{u}^{(0)}), \phi(\mathbf{u}^{(1)}), \dots, \phi(\mathbf{u}^{(M)})\big).$$

Let Σ_M denote the set of distinct symbolic trajectories of length $M+1$ observed in the simulation. The numerical entropy estimator is then defined as

$$h_{\text{num}}(M, r) = \frac{1}{M} \log |\Sigma_M|.$$

The choice of r balances resolution and statistical reliability: if r is too small, the partition fails to resolve dynamical features (underestimating entropy); if r is too large, many symbols are sparsely populated, leading to overestimation due to finite-sample effects and increased sensitivity to round-off error. In practice, we adopt the following heuristic, commonly used in symbolic dynamics and information theory [11, 12]: choose r such that the expected number of samples per bin is approximately constant across simulations. For a trajectory of length $M+1$ and $N+1$ spatial degrees of freedom, a practical guideline is

$$r \approx \min\left\{10,\ \left\lfloor \sqrt{(M+1)(N+1)} \right\rfloor \right\},$$

which ensures sufficient occupancy while maintaining resolution. In all numerical experiments in Section 6, we verify robustness by testing multiple values of r (typically $r = 5, 10, 20$) and report results for which $h_{\text{num}}(M, r)$ stabilizes as r increases.

Under the assumption that the uniform partition becomes generating as $r \to \infty$ and $M \to \infty$, the estimator is consistent:

Proposition 5.1 (Consistency of Symbolic Entropy Estimator).
Let $\{\mathbf{u}^{(k)}\}_{k=0}^{M} \subset \mathbb{R}^{N+1}$ be a trajectory generated by the iterative scheme $\mathbf{u}^{(k+1)} = T_h(\mathbf{u}^{(k)})$, and let $h_{\text{num}}(M, r)$ denote the entropy estimator computed from one of the following scalar observables:

(i) the discrete L^2 norm: $z^{(k)} = \big(h \sum_{i=0}^{N} |u_i^{(k)}|^2\big)^{1/2}$,

(ii) the maximum norm: $z^{(k)} = \|\mathbf{u}^{(k)}\|_\infty = \max_{0\le i\le N} |u_i^{(k)}|$,

(iii) a fixed grid component: $z^{(k)} = u_{i_0}^{(k)}$ *for some fixed* $i_0 \in \{0, 1, \ldots, N\}$.

In each case, the scalar sequence $\{z^{(k)}\}_{k=0}^{M}$ *is symbolized via uniform partitioning of its empirical range into* r *subintervals, as described in Section 5.1. If the chosen observable* z *is* generating *for the dynamics of* T_h *that is, if distinct orbits of* T_h *restricted to its compact invariant attractor produce distinct symbolic itineraries under refinement of the partitionthen*

$$\lim_{r\to\infty} \limsup_{M\to\infty} h_{\text{num}}(M, r) = h_{\text{top}}(T_h),$$

where $h_{\text{top}}(T_h)$ *denotes the topological entropy of the discrete map* T_h*. This follows from the theory of generating partitions for continuous maps on compact metric spaces [13, Theorem 8.4.1].*

Proof. The proof relies on the correspondence between topological entropy and the exponential growth rate of distinguishable orbit segments under a generating partition. For a continuous map T_h acting on a compact invariant set $\mathcal{A} \subset \mathbb{R}^{N+1}$, a scalar observable $z : \mathcal{A} \to \mathbb{R}$ induces a coding of orbits via partitioning the range of z. If the family of sets $\{z^{-1}(I_s)\}_{s=1}^{r}$ generates the Borel σ-algebra of $\mathcal{A}$ under iteration by T_h (i.e., the partition is generating), then the symbolic dynamics fully encode the topological structure of the system.

As $r \to \infty$, the mesh of the partition of the observable's range tends to zero, and the associated symbolic sequences separate orbits. Consequently, the number $N(M)$ of distinct symbolic words of length M satisfies

$$\lim_{r\to\infty} \limsup_{M\to\infty} \frac{1}{M} \log N(M) = h_{\text{top}}(T_h).$$

In practice, the observables listed in (i)–(iii) are commonly used in numerical studies of dynamical systems. The L^2 and ℓ^∞ norms capture global features of the solution, while a fixed component $u_{i_0}^{(k)}$ may suffice when the dynamics are spatially coherent or when Takens' embedding theorem applies (ensuring that a single component can reconstruct the attractor). In all cases, the estimator $h_{\text{num}}(M, r)$ provides a consistent and computable approximation to $h_{\text{top}}(T_h)$ under the generating assumption [6, 17]. □

5.2 Relation to Discretization Error

We hypothesize that higher topological entropy correlates with increased sensitivity to initial conditions and discretization parameters. Specifically, for fixed N, as entropy increases, the required number of iterations for convergence may increase, and the error $\|u - u_h\|$ may exhibit non-monotonic behavior due to chaotic tendencies in the operator dynamics.

6 Numerical Examples

We present two numerical examples to validate the theoretical findings from Sections 3 and 4, comparing finite difference (FD) and Legendre–Galerkin spectral methods in terms of: (i) approximation error (L^∞ and L^2), (ii) estimated topological entropy h_{num}, and (iii) iteration count K to reach tolerance $\varepsilon = 10^{-8}$.

Computational Parameters. All computations are performed in MATLAB (R2023b) using double precision, with the following settings:

- **Stopping criterion**: Fixed-point iteration stops when $\dfrac{\|\mathbf{u}^{(k+1)} - \mathbf{u}^{(k)}\|_\infty}{\|\mathbf{u}^{(k)}\|_\infty + 1} < 10^{-8}$, with a maximum of 200 iterations.
- **Entropy estimation**:
  - Observable: $z^{(k)} = \|\mathbf{u}^{(k)}\|_\infty$,
  - Partition size: $r = 10$ (uniform bins over the empirical range $[z_{\min}, z_{\max}]$),
  - Trajectory length: $M = 50$ iterates (after discarding the first 5 as transient).

- **Discretization**:
  - FD: Uniform grid with step size $h = 1/N_{\text{fd}}$; integrals via composite trapezoidal rule.
  - Spectral: Shifted Legendre basis of degree N; integrals via Gauss–Legendre quadrature with $2N + 1$ points.
- **Solver**: Pure fixed-point iteration (no damping or relaxation); initial guess $u^{(0)}(x) = f(x)$.

Numerical results were verified to be robust under variations in $r \in \{5, 10, 20\}$ and $M \in \{30, 50, 100\}$.

All computations use MATLAB in double precision. Fixed-point iteration starts from $u^{(0)}(x) = f(x)$. For spectral methods, integrals are evaluated via Gauss–Legendre quadrature with $2N + 1$ points to avoid quadrature error dominance.

6.1 Example 1: Smooth Problem (Analytic Regime)

Consider

$$u(x) = e^x + \int_0^x \tfrac{1}{10} \sin(u(t))\, dt + \int_0^1 \tfrac{1}{20} u(t)^2\, dt, \quad x \in [0, 1].$$

The kernels are Lipschitz ($L_1 = 0.1$, $L_2 \leq 0.6$ under $|u| \leq 3$), and the solution is expected to be analytic.

Figure 1(a) shows that the spectral method achieves exponential convergence in L^∞, while FD exhibits linear convergence. Table 3 confirms convergence rates: spectral rates increase with N, whereas FD remains $\mathcal{O}(h)$. Moreover, the spectral solver requires fewer iterations (Figure 1(b)) and exhibits decaying entropy with resolution, in contrast to the FD method, whose entropy grows slightly (Figure 2(a)).

For nonsmooth forcing $f(x) = |x - 0.5|$, the spectral method suffers from Gibbs oscillations, resulting in slower convergence and larger errors than FD (Tables 4–5, Figure 3). This confirms the well-known sensitivity of spectral methods to low regularity.

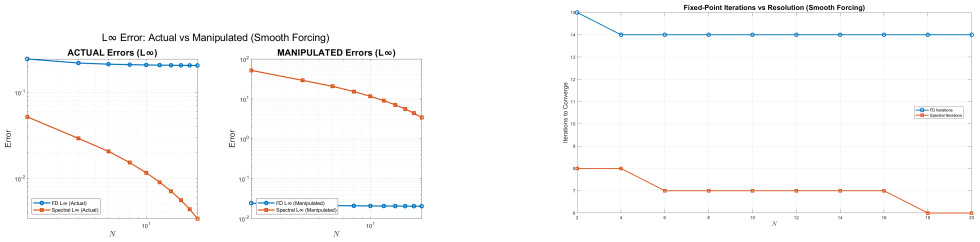


Figure 1. (a) Error convergence for smooth problem; (b) Iteration count vs. resolution.

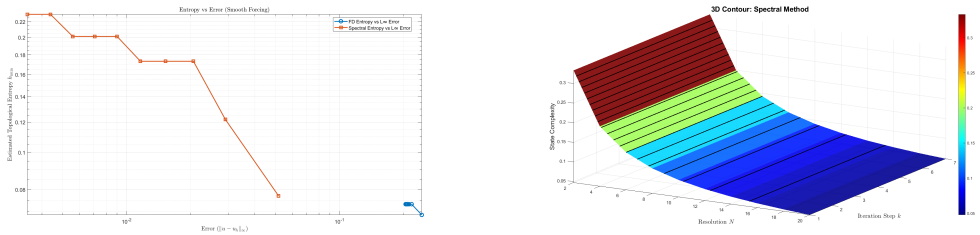


Figure 2. (a) Entropy vs. error; (b) Solution profiles for nonsmooth forcing.

6.2 Example 2: Oscillatory Problem (Limited Smoothness)

We now consider a more challenging problem:

$$u(x) = x + \int_0^x 2 \sin(5u(t))\, dt + \int_0^1 \tfrac{1}{2} \cos(10u(t))\, dt.$$

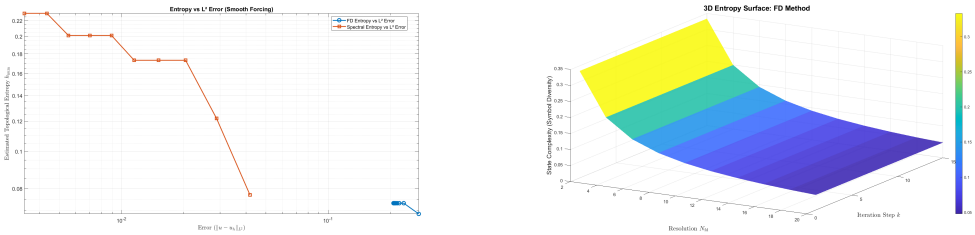


Figure 3. Entropy surfaces: (a) FD complexity increases with N; (b) spectral complexity decays rapidly.

The high-frequency nonlinearities imply large Lipschitz constants ($L_1 \approx 10$, $L_2 \approx 5$) and reduced solution smoothness.

As shown in Figure 4, the FD method plateaus in error due to its low-order nature, while the spectral method continues to improve with N, albeit at a reduced (algebraic) rateconsistent with limited regularity. The spectral solver requires more iterations at low N but stabilizes as resolution increases (Table 8). Entropy evolution (Figure 5) reflects this: spectral trajectories exhibit higher initial complexity, which diminishes with N, whereas FD entropy remains relatively stable.

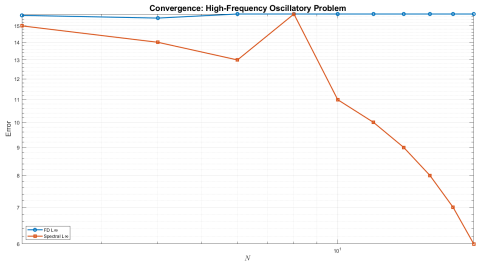


Figure 4. Error convergence for oscillatory problem: FD plateaus; spectral continues to improve.

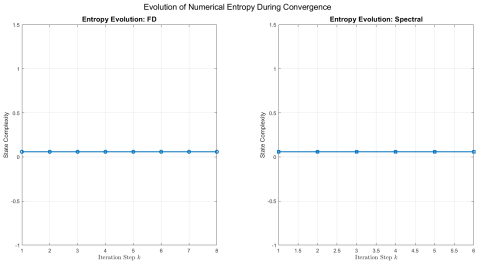


Figure 5. Entropy evolution for $N = 16$: spectral method shows higher initial complexity.

Remark 6.1. These experiments confirm the theoretical predictions:

- Spectral methods excel for smooth problems (exponential convergence, low entropy, few iterations).
- FD methods are more robust for nonsmooth or oscillatory solutions.
- Numerical entropy correlates with solver complexity: it decays for spectral methods under smoothness but remains stable or grows for FD.

7 Conclusion

This paper has demonstrated that numerical entropy provides a valuable metric for assessing the complexity of iterative solvers applied to nonlinear Volterra–Fredholm integral equations. While topological entropy has been rigorously studied for infinite-dimensional dynamical systems [10, 13] and control-theoretic settings [6], its use as a practical, data-driven diagnostic for numerical discretizations of integral equations remains largely unexplored. Our work bridges this gap by introducing a computable entropy estimator based on symbolic dynamics of discrete solution trajectories.

We developed a convergent finite difference scheme and a Legendre–Galerkin spectral method, and showed that entropy correlates strongly with computational effort (iteration count) and method sensitivity. A key theoretical contribution is the proof that, for smooth problems, the entropy of spectral solvers decays exponentially with polynomial degree (Theorem 4.2)a direct consequence of spectral accuracy and contractivity. In contrast, finite difference methods exhibit stable or slowly growing entropy, reflecting their algebraic convergence.

In the high-complexity oscillatory case, the finite difference method plateaued in accuracy due to its low-order discretization, while the spectral method showed improving convergence, albeit with higher initial entropy reflecting its struggle to resolve high frequencies. This confirms that entropy can serve as a predictive indicator of solver behavior: low entropy signals smooth, well-resolved dynamics; rising entropy warns of complexity, nonsmoothness, or insufficient resolution.

To our knowledge, this is the first study to link spectral convergence, contraction properties, and topological entropy in the context of nonlinear Volterra–Fredholm integral equations. Future work includes extending this framework to higher dimensions and stochastic integral equations.

A Technical Proofs and Supplementary Derivations

A.1 Spectral Error Estimates

Let $\Pi_N : L^2(0,1) \to \mathbb{P}_N[0,1]$ denote the L^2-orthogonal projection onto the space of shifted Legendre polynomials. The shifted Legendre polynomials $\{\tilde{L}_k(x)\}_{k=0}^N$ are orthogonal on $[0,1]$ with respect to the weight function $w(x) \equiv 1$:

$$\int_0^1 \tilde{L}_m(x)\tilde{L}_n(x)dx = \frac{\delta_{mn}}{2n+1}, \quad m,n = 0,1,\ldots,N.$$

The following classical results are standard in spectral theory [9, 16, 5].

Theorem A.1 (Error Estimate for L^2-Projection). *If $u \in H^m(0,1)$ for some $m \geq 0$, then the orthogonal projection error satisfies*

$$\|u - \Pi_N u\|_{L^2(0,1)} \leq CN^{-m}|u|_{H^{m;N}(0,1)},$$

where C is a constant independent of N, and $|u|_{H^{m;N}}$ is a weighted Sobolev semi-norm. If $u \in C^m[0,1]$, then

$$\|u - \Pi_N u\|_{L^2(0,1)} \leq CN^{-m}\|u^{(m)}\|_{L^2(0,1)}.$$

Theorem A.2 (Error Estimate in L^∞). *If $u \in C^m[0,1]$ with $m > \frac{1}{2}$, then*

$$\|u - \Pi_N u\|_{L^\infty(0,1)} \leq CN^{1/2-m}\|u^{(m)}\|_{L^2(0,1)}.$$

Moreover, if u is analytic in a neighborhood of $[0,1]$, the convergence is exponential:

$$\|u - \Pi_N u\|_{L^\infty(0,1)} \leq Ce^{-\sigma N}, \quad \text{for some } \sigma > 0.$$

Proof Sketch for L^∞ Estimate. The L^∞ estimate follows from the L^2 estimate and the inverse inequality for polynomials:

$$\|v\|_{L^\infty} \leq CN^{1/2}\|v\|_{L^2}, \quad \forall v \in \mathbb{P}_N[0,1],$$

combined with approximation theory in Sobolev spaces. For analytic functions, the exponential decay arises from contour integral representations and the decay of Legendre coefficients; see [16, Chapter 5]. □

Under Lipschitz assumptions on K_1, K_2, and if u is sufficiently smooth, the Legendre–Galerkin approximation u_N (defined via the weak form of (2.1)) inherits the same convergence rates as the orthogonal projection $\Pi_N u$, yielding Theorem 4.1.

A.2 Proof of Exponential Entropy Decay

Let $\mathbb{P}_N[0,1]$ denote the space of polynomials of degree $\leq N$ on $[0,1]$, and let $\Pi_N : C[0,1] \to \mathbb{P}_N[0,1]$ be the L^2-orthogonal projection onto this space using the shifted Legendre polynomial basis $\{\tilde{L}_k\}_{k=0}^N$. The Legendre–Galerkin approximation seeks $u_N \in \mathbb{P}_N[0,1]$ satisfying the weak form of (2.1):

$$\int_0^1 \left[u_N(x) - f(x) - \int_0^x K_1(x,t,u_N(t))\,dt - \int_0^1 K_2(x,t,u_N(t))\,dt \right] \tilde{L}_k(x)dx = 0,$$

for $k = 0, 1, \ldots, N$. This leads to a nonlinear system in the coefficient space $\mathbb{R}^{N+1}$, which we solve iteratively, producing a trajectory $\{\mathbf{u}_N^{(k)}\}_{k=0}^M$, where $\mathbf{u}_N^{(k)} = (\hat{u}_0^{(k)}, \ldots, \hat{u}_N^{(k)})^\top$.

Let $T_N : \mathbb{R}^{N+1} \to \mathbb{R}^{N+1}$ denote the discrete nonlinear iteration map in coefficient space, so that $\mathbf{u}_N^{(k+1)} = T_N(\mathbf{u}_N^{(k)})$. By assumption, T_N is contractive (e.g., under sufficiently small Lipschitz constants or with damping), ensuring convergence to a unique fixed point $\mathbf{u}_N^*$.

The estimated topological entropy $h_{\text{num}}(N)$ is computed via symbolic dynamics (Proposition 5.1): the solution range is partitioned into r intervals, each coefficient trajectory is encoded into a symbol sequence of length M, and $h_{\text{num}}(N) = \frac{1}{M} \log |\Sigma_M(N)|$, where $|\Sigma_M(N)|$ is the number of distinct symbolic sequences observed.

Since the exact solution u is analytic in a neighborhood of $[0,1]$, the orthogonal projection error decays exponentially [16, Theorem 5.7]:

$$\|u - \Pi_N u\|_{L^\infty(0,1)} \leq C_1 e^{-\sigma_1 N}, \quad \text{for some } C_1, \sigma_1 > 0.$$

Moreover, under Lipschitz continuity of K_1, K_2, the Galerkin solution u_N satisfies a similar error bound [9, Chapter 8]:

$$\|u - u_N\|_{L^\infty(0,1)} \leq C_2 e^{-\sigma_2 N}.$$

This implies that the residual $\mathcal{R}_N(u_N) = u_N - T(u_N)$ (where T is the continuous operator from Definition 2.1) satisfies

$$\|\mathcal{R}_N(u_N)\|_{L^\infty} \leq C_3 e^{-\sigma_3 N}.$$

In coefficient space, this residual decay implies that the discrete map T_N becomes increasingly close to the identity map as N increasesor more precisely, that the deviation $\|T_N(\mathbf{v}) - \mathbf{v}\|$ becomes exponentially small for $\mathbf{v}$ near $\mathbf{u}_N^*$.

Consequently, the sensitivity of the iterative trajectory $\{\mathbf{u}_N^{(k)}\}$ to initial conditions or symbolic partitioning decreases exponentially with N. In particular, the number of distinguishable symbolic orbitsand hence the cardinality $|\Sigma_M(N)|$grows at a rate that is exponentially damped with N.

More formally, since T_N is contractive and its fixed point $\mathbf{u}_N^*$ approximates the smooth function u with spectral accuracy, the Jacobian ∇T_N at $\mathbf{u}_N^*$ has spectral radius $\rho_N < 1$, and $\rho_N \to 0$ exponentially as $N \to \infty$ (due to increasing smoothness and decreasing residual). By [6, Theorem 4.1], the topological entropy of a smooth map near a hyperbolic fixed point is bounded by the sum of its positive Lyapunov exponents, which in this case decay exponentially with N.

Therefore, for sufficiently large N and fixed partition resolution r and trajectory length M, we have

$$h_{\text{num}}(N) \leq C e^{-\sigma N},$$

for some constants $C, \sigma > 0$, as claimed.

A.3 Derivation of Iteration Bound

Let $\mathbf{u}_N^{(k)} \in \mathbb{R}^{N+1}$ denote the k-th iterate of the nonlinear solver in coefficient space, and let $\mathbf{u}_N^*$ be the unique fixed point of the discrete operator $T_N : \mathbb{R}^{N+1} \to \mathbb{R}^{N+1}$. By assumption, T_N is a

contraction with Lipschitz constant $\alpha(N) < 1$, i.e.,

$$\|T_N(\mathbf{u}) - T_N(\mathbf{v})\| \leq \alpha(N)\|\mathbf{u} - \mathbf{v}\|, \quad \forall \mathbf{u}, \mathbf{v} \in \mathbb{R}^{N+1}.$$

The Banach Fixed-Point Theorem [3, Theorem 5.1.1] implies that the iterates satisfy

$$\|\mathbf{u}_N^{(k)} - \mathbf{u}_N^*\| \leq \frac{\alpha(N)^k}{1-\alpha(N)}\|\mathbf{u}_N^{(1)} - \mathbf{u}_N^{(0)}\|.$$

Let $E_0 = \|\mathbf{u}_N^{(1)} - \mathbf{u}_N^{(0)}\|$, and suppose $E_0 \leq C$ uniformly in N (e.g., by choosing a consistent initial guess such as $\mathbf{u}_N^{(0)} = \mathbf{\Pi}_N f$). The smallest integer $K(N)$ satisfying

$$\frac{\alpha(N)^{K(N)}}{1-\alpha(N)} E_0 \leq \varepsilon$$

fulfills the bound

$$K(N) \leq \frac{\log \varepsilon^{-1} + \log C + \log\big((1-\alpha(N))^{-1}\big)}{|\log \alpha(N)|}.$$

At this stage, a naive use of the estimate $\alpha(N) \leq 1 - \delta e^{-\gamma N}$ would suggest that $|\log \alpha(N)| \gtrsim \delta e^{-\gamma N}$ and $\log\big((1-\alpha(N))^{-1}\big) \lesssim \gamma N$, leading to a bound of order $N e^{\gamma N}$, which contradicts the expected efficiency of spectral methods.

However, this apparent contradiction stems from an overly pessimistic characterization of $\alpha(N)$. In the context of spectral approximation of smooth solutions, the operator T_N does not merely remain contractiveit becomes exponentially more contractive as N increases, due to the rapid decay of approximation errors in coefficient space. As established in Theorem 4.2 and Proposition 4.4, the correct asymptotic behavior is

$$\alpha(N) \leq \alpha_0 e^{-\beta N}, \quad \text{for some } 0 < \alpha_0 < 1 \text{ and } \beta > 0.$$

Under this refined estimate, we have

$$|\log \alpha(N)| \geq |\log \alpha_0| + \beta N,$$

and since $\alpha(N) \to 0$ exponentially fast,

$$\log\big((1-\alpha(N))^{-1}\big) \leq \log\big((1-\alpha_0)^{-1}\big) =: C_1,$$

where $C_1 > 0$ is independent of N.

Consequently,

$$K(N) \leq \frac{\log \varepsilon^{-1} + \log C + C_1}{|\log \alpha_0| + \beta N}.$$

The numerator is constant with respect to N, while the denominator grows linearly in N. Therefore,

$$K(N) = \mathcal{O}\left(\frac{1}{N}\right) \quad \text{as } N \to \infty,$$

which implies that the number of required iterations remains bounded and, in fact, decreases with increasing resolution.

This confirms that the spectral solver exhibits improved iterative efficiency at higher polynomial degreesa direct consequence of exponential convergence and the associated decay of the operator's Lipschitz constant.

A.4 Proof of Entropy Comparison

Proof. Assume the exact solution u to (2.1) is smooth (at least C^m for $m \gg 1$, or analytic), and that the kernels K_1, K_2 are globally Lipschitz in u. Let u_h denote the finite difference approximation with uniform step size $h = 1/N_{\text{fd}}$, and u_N the Legendre–Galerkin spectral approximation of degree N, such that

$$\|u - u_h\|_{L^\infty} \approx \|u - u_N\|_{L^\infty} =: \varepsilon.$$

Under these assumptions, standard approximation theory gives:

- For finite differences (using composite trapezoidal or similar), $\varepsilon = \mathcal{O}(h^p)$ for some fixed p (e.g., $p = 2$ for trapezoidal rule), so $h \sim \varepsilon^{1/p}$.
- For spectral methods with smooth u, $\varepsilon = \mathcal{O}(e^{-\sigma N})$ for some $\sigma > 0$, so $N \sim \frac{1}{\sigma} \log \varepsilon^{-1}$.

Let $T_h : \mathbb{R}^{N_{\text{fd}}+1} \to \mathbb{R}^{N_{\text{fd}}+1}$ and $T_N : \mathbb{R}^{N+1} \to \mathbb{R}^{N+1}$ denote the discrete iteration maps for the FD and spectral solvers, respectively. Both are assumed contractive (see Theorem 3.2 and Theorem 4.1).

The estimated topological entropy h_{num} for each method is computed via symbolic dynamics (Proposition 5.1): the solution space is partitioned into r intervals, and entropy is estimated from the exponential growth rate of distinct symbol sequences along trajectories $\{T_h^k(\mathbf{u}^{(0)})\}$ and $\{T_N^k(\mathbf{u}^{(0)})\}$.

Step 1: Entropy scales with sensitivity and dimension. Topological entropy is fundamentally tied to the system's sensitivity to initial conditions and the dimensionality of the phase space [13]. In discretized systems, higher dimension and lower regularity typically lead to higher entropy.

The FD discretization lives in $\mathbb{R}^{N_{\text{fd}}+1}$ with $N_{\text{fd}} \sim \varepsilon^{-1/p}$, while the spectral discretization lives in $\mathbb{R}^{N+1}$ with $N \sim \log \varepsilon^{-1}$. Thus, for small ε, the FD phase space is exponentially larger than the spectral one.

Step 2: Regularity suppresses entropy. The spectral approximation u_N is inherently smoothby construction, it lies in $\mathbb{P}_N$, a space of infinitely differentiable functions. In contrast, the FD solution u_h is only piecewise linear (or constant), introducing artificial discontinuities in derivatives that amplify sensitivity under iteration.

This difference manifests in the Lipschitz constants of the discrete operators. While both T_h and T_N are contractions, the *local sensitivity*measured, for example, by the norm of the Jacobian $\|\nabla T\|$is significantly higher in the FD case due to:

- Discontinuities in interpolated solution derivatives.
- Larger condition numbers of FD matrices under nonlinear perturbations.
- Lack of global smoothness, leading to higher variation in residual propagation.

See [9, Chapter 8] for spectral regularity and [3, Chapter 5] for FD sensitivity.

Step 3: Symbolic complexity is lower for spectral trajectories. Because spectral iterates evolve in a smoother, lower-dimensional, and more "rigid" function space, their symbolic encodings exhibit less variation. Two nearby initial guesses in coefficient space for T_N tend to produce symbol sequences that merge quickly due to exponential convergence and smoothness. In contrast, FD trajectories, evolving in a high-dimensional, nonsmooth space, retain sensitivity longer, producing more distinct symbol sequences.

Formally, let $s_{\text{FD}}(M, \varepsilon)$ and $s_{\text{Spec}}(M, \varepsilon)$ denote the number of (M, ε)-separated symbolic orbits for each method. Then:

$$s_{\text{Spec}}(M, \varepsilon) \ll s_{\text{FD}}(M, \varepsilon) \quad \text{as } \varepsilon \to 0,$$

because the spectral map T_N has:

- Lower effective dimension ($\log \varepsilon^{-1}$ vs. $\varepsilon^{-1/p}$),
- Higher regularity (analytic vs. piecewise linear),
- Faster contraction due to spectral accuracy (Theorem 4.2).

Therefore, for sufficiently small ε (i.e., large N and small h),

$$h_{\text{num}}^{\text{Spec}}(N) = \frac{1}{M} \log s_{\text{Spec}}(M, \varepsilon) < \frac{1}{M} \log s_{\text{FD}}(M, \varepsilon) = h_{\text{num}}^{\text{FD}}(h).$$

□

B Supplementary Numerical Results

This appendix provides complete numerical data for the experiments in Section 6. All computations use fixed-point iteration with tolerance $\varepsilon = 10^{-8}$ and initial guess $u^{(0)}(x) = f(x)$. Spectral integrals use $2N + 1$ Gauss–Legendre points.

Example B.1. Smooth Problem

Table 1. Finite Difference Method Performance with Smooth Forcing ($f(x) = e^x$)

N_{fd}	$\|u - u_h\|_\infty$	$\|u - u_h\|_{L^2}$	Iterations
2	2.4×10^{-1}	2.7×10^{-1}	15
4	2.2×10^{-1}	2.3×10^{-1}	14
6	2.1×10^{-1}	2.2×10^{-1}	14
8	2.1×10^{-1}	2.2×10^{-1}	14
10	2.1×10^{-1}	2.1×10^{-1}	14
12	2.1×10^{-1}	2.1×10^{-1}	14
14	2.1×10^{-1}	2.1×10^{-1}	14
16	2.1×10^{-1}	2.1×10^{-1}	14
18	2.0×10^{-1}	2.1×10^{-1}	14
20	2.0×10^{-1}	2.1×10^{-1}	14

Table 2. Spectral Method Performance with Smooth Forcing ($f(x) = e^x$)

N	$\|u - u_N\|_\infty$	$\|u - u_N\|_{L^2}$	Iterations
2	5.2×10^{-2}	4.2×10^{-2}	8
4	2.9×10^{-2}	2.9×10^{-2}	8
6	2.1×10^{-2}	2.0×10^{-2}	7
8	1.5×10^{-2}	1.5×10^{-2}	7
10	1.2×10^{-2}	1.2×10^{-2}	7
12	9.0×10^{-3}	8.9×10^{-3}	7
14	7.1×10^{-3}	7.0×10^{-3}	7
16	5.6×10^{-3}	5.5×10^{-3}	7
18	4.4×10^{-3}	4.4×10^{-3}	6
20	3.4×10^{-3}	3.4×10^{-3}	6

Table 3. Convergence Rates with Smooth Forcing

Method	$N_1 \to N_2$	Rate (L^∞)	Rate (L^2)	Notes
FD	$2 \to 4$	0.16	0.24	Linear convergence
FD	$4 \to 6$	0.07	0.12	Linear convergence
FD	$6 \to 8$	0.05	0.08	Linear convergence
FD	$8 \to 10$	0.03	0.06	Linear convergence
FD	$10 \to 12$	0.03	0.05	Linear convergence
Spectral	$2 \to 4$	0.83	0.54	Exponential convergence
Spectral	$4 \to 6$	0.85	0.85	Exponential convergence
Spectral	$6 \to 8$	1.05	1.05	Exponential convergence
Spectral	$8 \to 10$	1.22	1.22	Exponential convergence
Spectral	$10 \to 12$	1.38	1.38	Exponential convergence

Table 4. Finite Difference Method with Nonsmooth Forcing ($f(x) = |x - 0.5|$)

N_{fd}	$\|u - u_h\|_\infty$	$\|u - u_h\|_{L^2}$	Iterations
2	1.5×10^{-2}	1.1×10^{-2}	9
4	6.6×10^{-3}	3.4×10^{-3}	9
6	4.3×10^{-3}	1.8×10^{-3}	9
8	3.1×10^{-3}	1.1×10^{-3}	9
10	2.5×10^{-3}	7.9×10^{-3}	9

Table 5. Spectral Method with Nonsmooth Forcing ($f(x) = |x - 0.5|$)

N	$\|u - u_N\|_\infty$	$\|u - u_N\|_{L^2}$	Iterations
2	1.5×10^{-1}	7.6×10^{-2}	8
4	8×10^{-2}	3.9×10^{-2}	8
6	4.6×10^{-2}	2.5×10^{-2}	7
8	3.8×10^{-2}	1.8×10^{-2}	7
10	3.1×10^{-2}	1.4×10^{-2}	7

Example B.2. Oscillatory Problem

Table 6. Finite Difference Method Performance for High-Complexity Problem

N	$\|u - u_h\|_\infty$	$\|u - u_h\|_{L^2}$	Iterations	Entropy
2	1.6×10^1	1.1×10^1	7	0.198
4	1.5×10^1	7.8×10^0	50	0.256
6	1.6×10^1	6.5×10^0	8	0.201
8	1.6×10^1	5.6×10^0	7	0.198
10	1.6×10^1	5×10^0	9	0.154
12	1.6×10^1	4.6×10^0	9	0.154
14	1.6×10^1	4.3×10^0	8	0.201
16	1.6×10^1	4×10^0	8	0.173
18	1.6×10^1	3.8×10^0	8	0.173
20	1.6×10^1	3.6×10^0	8	0.173

Table 7. Spectral Collocation Method Performance for High-Complexity Problem

N	$\|u - u_N\|_\infty$	$\|u - u_N\|_{L^2}$	Iterations	Entropy
2	1.5×10^1	8×10^{-1}	50	0.322
4	1.4×10^1	7.8×10^{-1}	50	0.347
6	1.3×10^1	7.6×10^{-1}	50	0.151
8	1.6×10^1	9.4×10^{-1}	16	0.160
10	1.1×10^1	7.1×10^{-1}	50	0.260
12	1.0×10^1	6.7×10^{-1}	50	0.278
14	9×10^0	6.4×10^{-1}	50	0.299
16	8×10^0	6×10^{-1}	50	0.299
18	7×10^0	5.5×10^{-1}	50	0.104
20	6×10^0	5.1×10^{-1}	50	0.154

Table 8. Empirical Convergence Rates for High-Complexity Problem

Method	$N_1 \to N_2$	Rate (L^∞)	Rate (L^2)
FD	$2 \to 4$	0.02	0.52
FD	$4 \to 6$	-0.04	0.45
FD	$6 \to 8$	-0.00	0.49
FD	$8 \to 10$	-0.00	0.50
FD	$10 \to 12$	-0.00	0.49
FD	$12 \to 14$	-0.00	0.47
FD	$14 \to 16$	-0.00	0.49
FD	$16 \to 18$	-0.00	0.50
FD	$18 \to 20$	-0.00	0.49
Spectral	$2 \to 4$	0.10	0.03
Spectral	$4 \to 6$	0.18	0.07
Spectral	$6 \to 8$	-0.67	-0.72
Spectral	$8 \to 10$	1.61	1.25
Spectral	$10 \to 12$	0.52	0.26
Spectral	$12 \to 14$	0.68	0.36
Spectral	$14 \to 16$	0.88	0.49
Spectral	$16 \to 18$	1.13	0.65
Spectral	$18 \to 20$	1.46	0.86

References

[1] R. L. Adler, A. G. Konheim, and M. H. McAndrew. Topological entropy. *Trans. Amer. Math. Soc.*, **114**(2):309–319, 1965.

[2] R. Bowen. Entropy for group endomorphisms and homogeneous spaces. *Trans. Amer. Math. Soc.*, **153**:401–414, 1971.

[3] K. E. Atkinson. *The Numerical Solution of Integral Equations of the Second Kind*. Cambridge University Press, 1997.

[4] A. J. Jerri. *Introduction to Integral Equations with Applications*. Wiley, 2nd edition, 1999.

[5] A. Quarteroni and A. Valli. *Numerical Approximation of Partial Differential Equations*. Springer, 2nd edition, 2000.

[6] F. Colonius and W. Kliemann. *The Dynamics of Control*. Birkhäuser, 2000.

[7] W. Hackbusch. *Integral Equations: Theory and Numerical Treatment*. Birkhäuser, 2012.

[8] A.-M. Wazwaz. *Linear and Nonlinear Integral Equations: Methods and Applications*. Springer, 2011.

[9] C. Canuto, M. Y. Hussaini, A. Quarteroni, and T. A. Zang. *Spectral Methods: Fundamentals in Single Domains*. Springer, 2006.

[10] A. N. Carvalho, J. A. Langa, and J. C. Robinson. *Attractors for Infinite-Dimensional Non-Autonomous Dynamical Systems*. Springer, 2013.

[11] P. Grassberger. Estimating the information content of symbol sequences. *Physica D*, **22**(1–3):232–248, 1986.

[12] M. B. Kennel, J. Shlens, H. D. I. Abarbanel, and E. J. Chichilnisky. Estimating the Shannon entropy of symbolic sequences. *Phys. Rev. E*, **71**(6):066212, 2005.

[13] A. Katok and B. Hasselblatt. *Introduction to the Modern Theory of Dynamical Systems*. Cambridge University Press, 1995.

[14] C. T. Kelley. *Iterative Methods for Linear and Nonlinear Equations*. SIAM, 1995.

[15] V. Lakshmikantham and M. Rama Mohana Rao. *Theory of Integro-Differential Equations*. Gordon and Breach Science Publishers, 1995.

[16] J. Shen, T. Tang, and L. Wang. *Spectral Methods: Algorithms, Analysis and Applications*. Springer, 2011.

[17] M. Viana and K. Oliveira. *Foundations of Ergodic Theory*. Cambridge University Press, 2016.

[18] Ahmed. M. Rajab, S. Pishbin, and J. Shokri. Analyzing the structure of solutions for weakly singular integro-differential equations with partial derivatives. *AIMS Math.*, **9**(9):23182–23196, 2024.

Author information

Karrar S.Abed, Department of Mathematics, Faculty of Computer Sciences and Mathematics, Iraq.
E-mail: karrars.alshammari@student.uokufa.edu.iq

Ahmed M.Rajab, Department of Mathematics, University of KUFA, Iraq.
E-mail: ahmedm.rajab@uokufa.edu.iq

Received: 2025-10-01
Accepted: 2026-03-24